ChemElectroChem

Research Article
doi.org/10.1002/celc.202400651

Chemistry Europe
European Chemical Societies Publishing

www.chemelectrochem.org

pH Dependence of Noble Metals Dissolution: Ruthenium

Mária Minichová,*[a, b] Tatiana Priamushko,[a] Matej Zlatar,[a, b] Karl J. J. Mayrhofer,[a, b] and Serhiy Cherevko*[a]

Ruthenium (Ru) or Ru-based catalysts are widely used in various electrochemical applications such as biosensors, ammonia synthesis, CO_2 reduction, electrolyzers, or fuel cells, operating at different conditions. While the activity of these catalysts is widely studied, works addressing stability are less common, especially in neutral or alkaline environments. Therefore, we evaluate a real-time potential-dependent dissolution of polycrystalline Ru via scanning flow cell coupled to inductively coupled plasma mass spectrometry in acidic, alkaline, and phosphate buffer electrolytes using relevant potential ranges. On top of the fundamental understanding of Ru's dissolution, a particular focus lies on oxygen evolution reaction (OER) due to its importance in various electrochemical applications. We show that the dissolution behavior of Ru during dynamic operation is well in line with the thermodynamic predictions (except dissolution due to Ru^{2+} formation) and unique compared to other noble metals (Pt, Au, Ir). While the dissolution of polycrystalline Ru is the highest in alkaline pH at the onset of OER (1.4 V_{RHE}), no stability issues are visible at potentials up to 0.85 V_{RHE} at all pHs. This work establishes a stability baseline for researchers implementing Ru-based catalysts.

1. Introduction

The climate crisis and the depletion of natural resources have created a need for technologies that employ renewable energy sources. Among many research fields, electrocatalysis has grown enormously in recent years in the hope of providing solutions to the upcoming energy challenges by operative electrolyzers and fuel cells. Some electrocatalysts, indeed, found their commercial application, but the search for more efficient, longer-lasting alternatives is not finished.[1–3] One of many open challenges in this research is to understand the reasons behind the enhanced behavior of already known catalysts and to find better catalysts in terms of activity and stability.

Ru is a catalyst used in various electrochemical applications. To name some, it can be used in biosensors,[4] ammonia synthesis (N_2 reduction),[5] carbon capture (CO_2 reduction), green hydrogen production (electrolyzers), and as an alternative to combustion engines (fuel cells). In fuel cell and electrolyzer applications, Ru-containing catalysts are widely used but still intensively studied catalysts in many reactions. Ru itself can be used in oxygen evolution reaction (OER),[6,7] hydrogen evolution reaction (HER),[8,9] or hydrogen oxidation reaction (HOR),[10,11] and alloyed with other (primary noble) metals in the oxidation of alcohols[12–15] and also again in all three mentioned reactions (OER, HER, and HOR).[16–21] While the majority of studies focus on catalytic activity and lack information on catalyst stability, few works only address the stability of Ru or Ru-based catalysts.

The findings on the behavior of Ru in an acidic environment are the following: Ru is oxidized in ambient air quickly and forms reversible or irreversible oxides when exposed to positive potentials, and it dissolves more than other noble metals.[22–25] The thorough studies of the dissolution of Ru and RuO_2 provide an understanding of the difference in stability of these two materials, possibly appearing simultaneously under specific conditions. While RuO_2 is relatively stable up to 1.3 V_{RHE}, the dissolution of metallic Ru can be expected even below 1 V_{RHE} in parallel to oxidation.[26,27] The stability of the most common Ru-based catalysts, PtRu and IrRu, is not very commonly addressed except for a few dissolution studies showing decreased stability compared to bare Pt and Ir catalysts.[28–33]

The stability reports of Ru in an alkaline environment focus primarily on OER, where the reaction conditions cause significant stability issues.[27,34] Nevertheless, some works report successful implementation of Ru even in alkaline or neutral environments.[35–37] Similarly, HER is often studied in alkaline or neutral environments,[38,39] but comprehensive stability reports are lacking. Ru-based catalysts in ammonia synthesis and biosensors also use alkaline and neutral pHs for electrocatalysis. In general, there is very little known about the stability of Ru throughout the whole pH spectrum. For instance, how does the stability of Ru change gradually with the pH, and what are the pH limitations when considering Ru as a catalyst for various applications? Can the stability of Ru during dynamic operation be predicted purely from thermodynamics and thus from the Pourbaix diagram?

Hence, in this work, we have focused on the evaluation of the stability of Ru by measuring its real-time potential-dependent dissolution, utilizing inductively coupled plasma mass

[a] M. Minichová, T. Priamushko, M. Zlatar, K. J. J. Mayrhofer, S. Cherevko
Forschungszentrum Jülich GmbH, Helmholtz Institute Erlangen-Nürnberg for Renewable Energy (IET-2), Cauerstr. 1, 91058 Erlangen, Germany
E-mail: m.minichova@fz-juelich.de
s.cherevko@fz-juelich.de

[b] M. Minichová, M. Zlatar, K. J. J. Mayrhofer
Department of Chemical and Biological Engineering, Friedrich-Alexander-Universität Erlangen-Nürnberg, Egerlanstr. 3, 91058 Erlangen, Germany

Supporting information for this article is available on the WWW under https://doi.org/10.1002/celc.202400651

spectrometry and the scanning flow cell (SFC-ICP-MS) with electrolytes of various pHs (acidic, alkaline, and phosphate buffer electrolytes). Buffered conditions were selected over unbuffered ones to minimize potential local pH fluctuations.[40] The electrochemical protocols were chosen thoroughly, bearing in mind Ru's rapid spontaneous oxidation and the potential limits of the creation of irreversible oxides on the Ru surface. The intention to cover more applications of Ru or Ru-based catalysts in both fuel cells and electrolyzers was manifested by using the wide range of potential and the preference to obtain metallic Ru over its oxides. A particular focus is dedicated to the OER due to its importance and implications in various other processes. Nevertheless, we do not limit ourselves solely to OER application, as this fundamental work concerning Ru stability could serve the electrocatalytic community in the future. This work is also part of the series of works entitled: "pH dependence of noble metals dissolution." The interested reader is referred to works including platinum,[41] gold,[42] and iridium.[40]

Experimental Section

Materials

Ruthenium (Ru) cube 6 mm, (99.9%, VWR), $HClO_4$ (70%, Suprapur®), HNO_3 (69%, Suprapur®), HCl (36%, Suprapur®), KOH (99.99%, EMSURE®), KH_2PO_4 (99.995%, Suprapur®) and K_2HPO_4 (99.99%, Suprapur®) were purchased from Merck and used without further purification. Ar (99.999%) and H_2 (99.999%) were purchased from Air Liquide Deutschland GmbH. Solutions were prepared using ultrapure water (18.2 MΩ, TOC <3 ppb) provided by a Merck Millipore MilliQ system.

Preparation of Ru Electrode and Electrolytes

The surface of Ru foil was pretreated before each measurement to diminish the influence of surface oxidation and enhance the reproducibility of measurements. Ru was first ground (2×SiC paper #4000, Struers) at 35 N for 30 s and subsequently polished using a polishing pad (MD-Mol, Struers) and diamond paste (DiaPro, Struers) at 15 N for 10 min by polishing machine (Struers LaboForce-100).[40] After mechanical treatment, Ru was sonicated in deaerated ultrapure water (S 30 Elmasonic) for 10 min and then immersed into concentrated HNO_3 for 5 min, followed by electrochemical reduction at -0.1 V_{RHE}.[43] Ru foil was kept vacuum-sealed before the described surface treatment. Phosphate buffer was used to prepare solutions with final pH 3, 5, 7, 9, and 11 by varying rations between KH_2PO_4 and K_2HPO_4 while maintaining a total concentration of phosphate species to 0.05 M. For pH 1 and 12.7, 0.1 M HClO4 and 0.05 M KOH were used, respectively.[40–42] The pH meter (Mettler Toledo, SevenExcellence™) was used to confirm the final value of pH. The exact composition of electrolytes is listed in Table S1. For simplicity, pH 12.7 will be rounded to 13 in the results and discussion part.

SFC-ICP-MS Measurements

A custom-designed, home-built scanning flow cell (SFC) with an opening defining the geometric surface area (0.00907 cm^2) was used for all electrochemical measurements at pH 1–12.7.[44] The pretreated Ru foil employed as the working electrode was connected with an XYZ translation stage (Physik Instrumente M-403), which allowed measurements of different areas on the electrode. The glassy carbon rod (HTW, Sigradur G) was used as the counter electrode, and the Ag/AgCl/3 M KCl electrode (Metrohm) was used as the reference electrode. The reference electrode was calibrated daily to the reversible hydrogen electrode (RHE) scale. The electrolyte in all the experiments was purged by argon to avoid air contamination. A peristaltic pump (Ismatec) was used to control the stable flow of the electrolyte. The SFC station, consisting of multiple instruments, was fully operated by custom-designed LabView software.[33] Gamry Reference [600] potentiostat was used to carry out two electrochemical protocols. Protocols started at -0.1 V_{RHE} to reduce surface oxides, followed by either 3 cyclic voltammograms (CVs) in protocol 1 (P1) or 3 potential jumps in protocol 2 (P2) with subsequently rising upper potential limits (UPL) to 1.0, 1.2, and 1.4 V_{RHE}. The reduction step in between CVs or jumps was again at -0.1 V_{RHE} and lasted 3 min. Potential jumps also lasted 3 min. Scan rates of CVs and ramps (after jumps) were 10 $mV\,s^{-1}$. The electrolyte from the SFC was introduced to an inductively coupled plasma mass spectrometer (ICP-MS) online by connecting the electrolyte outlet of the SFC, forming the so-called SFC-ICP-MS. The ICP-MS was calibrated daily by a four-point calibration slope made from standard solutions of ^{102}Ru, which contained the metal ions of interest in each concentration range (0–5 $\mu g\,L^{-1}$) and electrolyte with the pH of the interest (1, 3, 5, 7, 9, 11 or 12.7). ^{103}Rh (10 $\mu g\,L^{-1}$) served as the internal standard. The purged electrolyte flow rate of SFC-ICP-MS was controlled by the peristaltic pump of the ICP-MS (MP2 pump, Elemental Scientific) with an average flow rate of 3.6 ± 0.1 $\mu l\,s^{-1}$. The detection limit of Ru during the measurements was 0.034 ± 0.011 $ng\,cm^{-2}$ (calculated as 3 times the standard deviation from the signal obtained at baseline).

Treatment of Polycrystalline Ru Surface

Metalic Ru is quickly oxidized in ambient air or aqueous solutions due to its high oxophilicity.[22,45] Therefore, studying the electrochemical behavior and stability of purely metallic Ru can be challenging. Especially when measurements are commonly executed in aqueous solutions, and preparation of electrodes (e.g., mechanical surface treatment) also happens in air. In addition, this rapid oxidation of the Ru surface also limits the possibility of ex-situ XPS measurements to evaluate oxidative changes on the surface before and after the SFC-ICP-MS measurements. A quick way to estimate whether Ru is metallic is by forming a H_{upd} region during CVs. This region can also serve to describe surface processes or to calculate a surface area. However, as the adsorption of OH on Ru takes place at significantly lower potentials than on other noble metals[45] and thus partly overlaps with Ru's H_{upd} region,[43,46] using H_{upd} for a quantitative description of surface processes can be challenging. Still, for the purposes of monitoring cleanliness, it will be satisfactory.

Metallic Ru should be oxidized only reversibly below a UPL of 0.9–1.0 V_{RHE}.[26,43] The different surface preparations (grinding, polishing, HNO_3 immersion, and electrochemical reduction) can lead to varying surface oxides.[43] In order to record a Ru CV, which allows for the description of surface processes, we first tried to treat the surface mechanically (grinding and polishing) and apply different reduction potentials (none, -0.05 V_{RHE}, and -0.1 V_{RHE}) in an acidic environment. As shown in Figure S1, no difference was observed between CVs, but the H_{upd} region was not visible. As shown in Figure S2, a visible difference in the shape of the CV appeared after the addition of extra surface treatment (sonication and HNO_3 immersion) on top of mechanical and electrochemical ones. However, again, the H_{upd} region was still not visible.

In search of a proper surface treatment to obtain the H_{upd} region, we have conducted a series of electrochemical protocols combining electrochemical cleaning by triggering dissolution (20 CVs at scan rate 200 mV s^{-1} at higher UPL) and electrochemical reduction (without, with prior cleaning only, with both prior and after cleaning). Figure S3 summarises the series of protocols using cleaning with a UPL of 1.2 V_{RHE}. The shape of CVs looks similar, and H_{upd} is only slightly visible. The cleaning at an even higher UPL of 1.4 V_{RHE} in Figure S4 shows visible H_{upd}. We have also conducted the same series of surface cleaning experiments in alkaline pH. The same series of protocols are visible in Figure S5 and Figure S6. Here, both cleaning UPLs resulted in visible H_{upd}. Increased dissolution of Ru in an alkaline environment probably played a role in the ability to clean the surface oxides at lower UPL compared to the acidic environment.[27] A detailed description of all applied procedures in Figures S1–S6 is summarized in Table S2.

We have demonstrated that obtaining a Ru surface free of oxides can be a challenge, and the H_{upd} region of Ru can be obtained only after cleaning triggering dissolution, while this method is simultaneously also reported to create irreversible oxides on the surface, which is not a viable option for our study.[26] Therefore, we will omit the lack of H_{upd} region in Ru CV and accept some level of oxidation on the Ru surface for the following dissolution studies. We will, however, strictly follow extensive surface treatment such as grinding, polishing, sonication, HNO_3 immersion, and reduction at −0.1 V_{RHE} to ensure reproducibility. The potential will be kept reductive (−0.1 V_{RHE}) also in between studied CVs or jumps in the electrochemical protocols.

2. Results and Discussion

2.1. Dissolution During CVs

To study the effect of pH on Ru dissolution, we first use potentiodynamic conditions represented by CVs in SFC-ICP-MS experiments. We choose a gradual increase of potential with UPL of 1.0 V_{RHE} in a regime of reversible Ru oxidation, 1.2 V_{RHE} for the formation of a passivation layer of irreversible Ru oxides, and 1.4 V_{RHE} to mimic conditions of significant oxidation of the Ru surface and initial OER.[24,26] The applied protocol used for measurements in 7 different pH values (1, 3, 5, 7, 9, 11, 13) can be seen in Figure 1a. Dissolution profiles recorded by ICP-MS are shown in Figure 1b and Figure 1c on a logarithmic scale for better visibility. When the Ru electrode is approached by the SFC cell, a contact peak appears due to the first surface reduction of oxides.[22] Subsequently, two peaks appear in each CV during positive and negative sweeps (called anodic and cathodic, respectively). These peaks are individually integrated for each CV (Figure 1d–1f).

In the case of UPL 1.0 V_{RHE}, anodic dissolution increases up to the local maximum at pH 3, reaches the local minimum at pH 5, and then gradually increases by increasing pH, reaching the maximum at pH 13. This trend is not very clearly visible due to the size of error bars and all dissolved amounts being below 1 ng cm^{-2}. In accordance with the literature,[26] we do not observe dissolution due to the transition from Ru^0 to Ru^{2+} or Ru^{3+} at potentials below 0.9 V_{RHE}, which is expected to happen

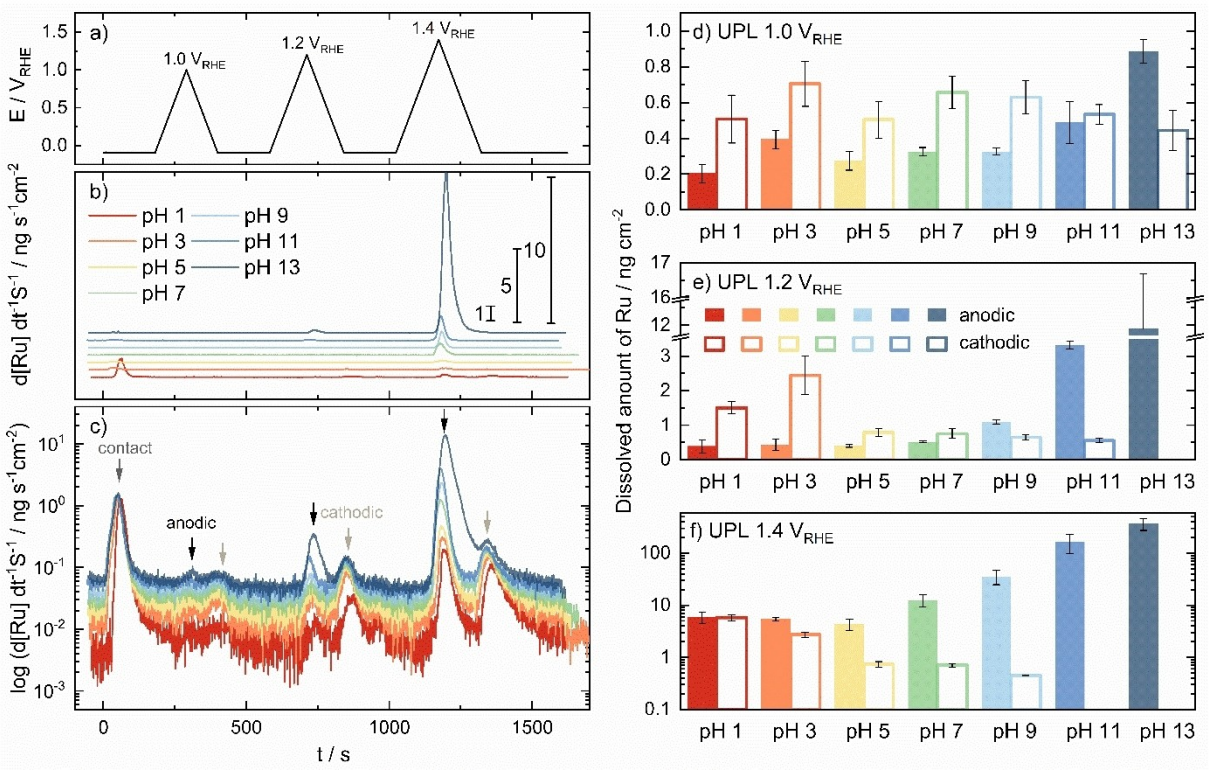

Figure 1. Dissolution of Ru in various pH during SFC-ICP-MS experiment in protocol 1 (P1). Electrochemical protocol consisting of 3 consecutive CVs (10 mV s^{-1}) starting at −0.1 V_{RHE} to 1.0, 1.2, and 1.4 V_{RHE} with reduction hold at −0.1 V_{RHE} before, after, and in between CVs in a), dissolution profiles in linear and logarithmic scale in b) and c), and integrated amounts of individual peaks at 1.0 V_{RHE} in d) at 1.2 V_{RHE} in e) and at 1.4 V_{RHE} in f).

thermodynamically (or we see this transition only at higher potential due to kinetic hindrance). This transition can be seen in the Pourbaix diagram (constructed at μM and nM equilibrium concentration of dissolved species) in Figure 2 or in the literature.[26,47] The reason for the absence of anodic dissolution at low potentials could be the presence of native oxides on the surface, similar to the case of Ir.[40] Instead, we most probably observe a transition to RuO_2 (at approximately 0.9 V_{RHE} in the Pourbaix diagram), considering that we do observe a dissolution peak in this region. As in the case of the anodic sweep, we do not observe any clear trend in the influence of pH on dissolution during the cathodic sweep. The observed peak in the cathodic sweep is most probably caused by the partial reduction of RuO_2, and we do not observe its dependence on pH.

The dissolution trends by pH are clearer at UPL 1.2 V_{RHE}. Anodic dissolution increases with rising pH, reaching an order of magnitude higher dissolution at pH 13 compared to pH 11. This is most probably caused by the same process (transition of $Ru(OH)_3$ to RuO_2). However, this time, the extent of oxidation is more pronounced due to higher UPL. Looking at Pourbaix diagrams at 1.2 V_{RHE}, RuO_4^{2-} starts to appear from pH 11 at μM concentration, and RuO_4^- (followed by RuO_4^{2-}) starts to appear from pH 7 at nM concentration. As these species are soluble and can thermodynamically exist at UPL 1.2 V_{RHE} in alkaline pH, we can assume that the existence of these soluble species can explain the increase of dissolution from pH 7 upwards. Cathodic dissolution, on the contrary, seems to have the opposite trend, and dissolution is generally higher at low pHs (1 and 3) compared to pH 13, where the cathodic peak completely vanishes. Reduction of RuO_2, therefore, seems to be still partly reversible up to pH 7, where we see reduction peaks higher than oxidation peaks. At higher pHs, this process alters and becomes more irreversible, probably due to the increased presence of soluble oxides and, thus, lower stability of RuO_2. The local increase of cathodic dissolution at pH 3 seems to be attributed to phosphates presence, which was also observed in the case of Ir.[40]

At UPL of 1.4 V_{RHE}, pH influence on Ru dissolution plays the biggest role. Therefore, Figure 1f needs to be shown on a logarithmic scale to visualize significant differences in dissolved amounts. The anodic dissolution again increases with pH, while cathodic dissolution decreases until it diminishes completely at pH 11 and 13. This trend seems to be only unique for Ru, as the other metals from the "pH study" series (Pt, Au, Ir) reached the minimum anodic and cathodic dissolution in neutral pH.[40–42] In an acidic environment (below pH 7), we most probably observe the transition of RuO_2–RuO_4 (H_2RuO_5) and the onset of dissolution due to OER,[26,27] which is also in line with the prediction from the Pourbaix diagram. In an alkaline environment, except for dissolution due to OER, the soluble RuO_4^{2-} exists. Again, the presence of soluble RuO_4^{2-} (or $H_2RuO_5^-$) can explain the reason for the significant increase in dissolution in alkaline pH. Looking at cathodic peaks, the only pH where we can consider this process partly reversible is pH 1, where the dissolved amounts during oxidation and reduction are equal. At UPL 1.4 V_{RHE}, the stability trend is clearly in favor of the acidic environment. All potential applications employing Ru-based

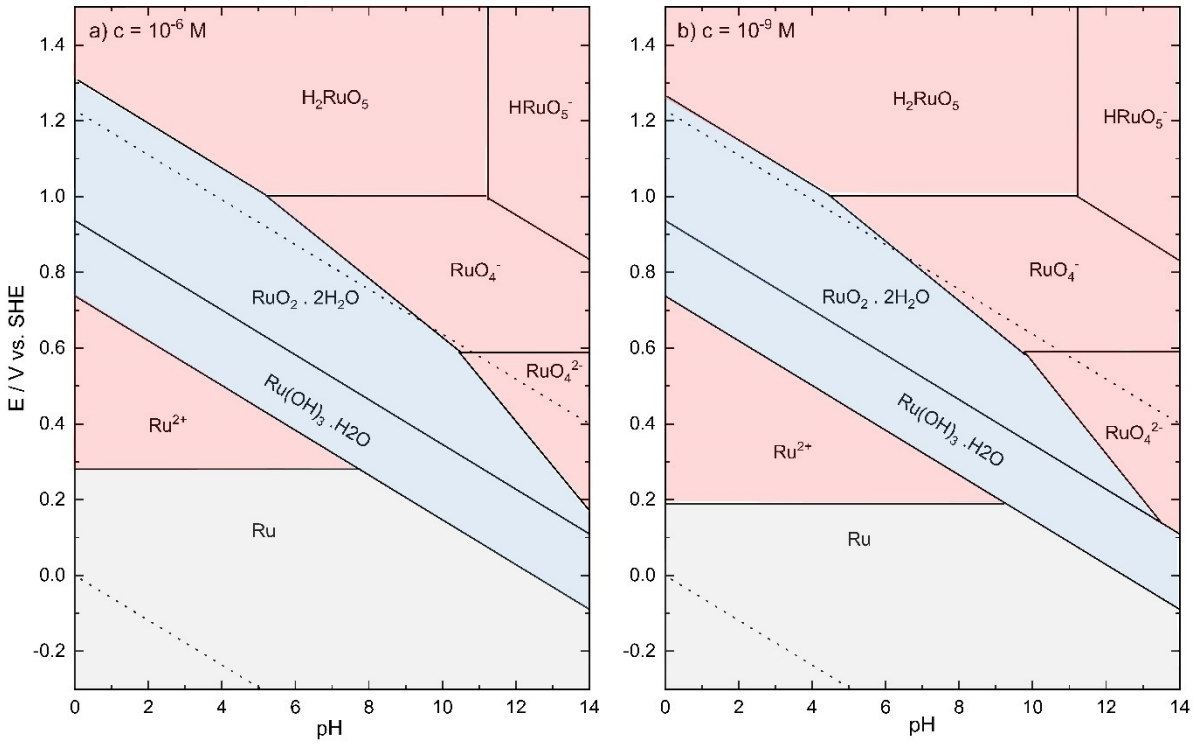

Figure 2. Pourbaix diagram of ruthenium calculated with an equilibrium concentration of 1 μM in a) and 1 nM in b). Equations used to construct the diagram are listed in Table S3 and taken from the literature.[48] Different colored areas represent the following: grey – a stable metallic region; blue – a region of stable oxides (hydroxides); and red – a region of dissolved (unstable) species.

catalysts in the alkaline environment in potential above 1.2 V_{RHE} should consider significant stability issues.

2.2. Dissolution During Potential Jumps

Contrary to CVs, potentiostatic experiments can capture steady-state conditions at a certain potential value and their effects on Ru dissolution in various pH values. As in the case of CVs, we have chosen the same UPLs for SFC-ICP-MS measurements and the same pH conditions. The electrochemical protocol, P2, is shown in Figure 3a, and the dissolution profiles on linear and logarithmic scales are shown in Figure 3b and Figure 3c. Dissolution peaks are again visible at the contact with the surface, then when triggered at each potential jump when the surface is oxidized and followed by a peak during the ramp (negative sweep) when the surface is reduced. Again, each peak is individually integrated, and the amounts are shown in Figures 3d–3f.

At UPL 1.0 V_{RHE}, anodic dissolution again increases up to the local maximum at pH 3, reaches the local minimum at pH 5, and then gradually increases by increasing pH, reaching the maximum at pH 13. This same trend as in P1 is more pronounced due to the higher total dissolved amounts caused by longer time exposure at UPL. Based on the Pourbaix diagram as concluded from P1, we most probably see the dissolution due to a transition to RuO_2. The trend in the cathodic dissolution also seems to be similar to that in P1, only more pronounced. The increased dissolution up to pH 3 drops at pH 5, followed by a gradual decrease with increasing pH. As the amount dissolved in the cathodic peak is higher in all pHs up to pH 11, it seems that RuO_2 formation is mostly reversible. Lastly, pH 3 seems to have a local maximum in dissolution amounts in both sweeps (especially cathodic). Therefore, it could be hypothesized that the higher dissolution could be caused by the introduction of phosphate buffer compared to a purely acidic environment at pH 1. A similar study shows that phosphate ions can adsorb on RuO_2 film without affecting the pH dependence of water electro-adsorption.[49] In addition, an increase in dissolution at pH 3 was also observed in the Ir study (a part of the series) and was correlated to phosphate buffer.[40]

At UPL 1.2 V_{RHE}, the dissolution trend during jumps for both anodic and cathodic dissolution is the same as during P1, but again with higher absolute amounts. In the case of UPL 1.4 V_{RHE}, anodic dissolution increases with pH gradually up to pH 11. It then slightly decreases at pH 13 (still having a higher amount than at pH 9), which is only a small deviation, and therefore, we can also assume the same trend. The cathodic dissolution at UPL 1.4 V_{RHE} follows the same trend as CVs in P1 as well. Overall, it can be concluded that the processes described in potentiodynamic conditions (P1) seem to also happen in steady-state conditions (P2) in all three studied UPLs.

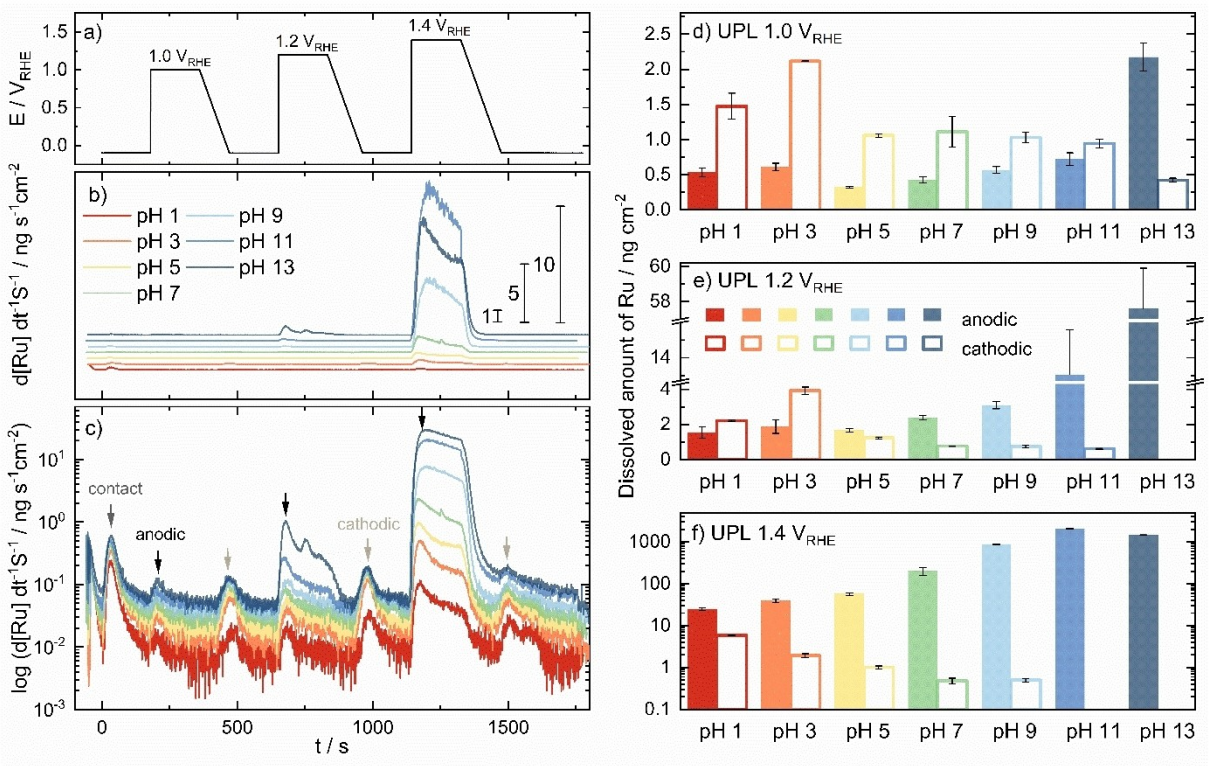

Figure 3. Dissolution of Ru in various pH during SFC-ICP-MS experiment in protocol 2 (P2). Electrochemical protocol consisting of 3 consecutive potential jumps to 1.0, 1.2, and 1.4 V_{RHE} followed by 3 min holds at these potentials and ramps (10 mV s^{-1}) back to −0.1 V_{RHE}, with reduction holds at −0.1 V_{RHE} before, after, and in between potential jumps in a), dissolution profiles in linear and logarithmic scale in b) and c), and integrated amounts of individual peaks at 1.0 V_{RHE} in d) at 1.2 V_{RHE} in e) and at 1.4 V_{RHE} in f).

2.3. Further Dissolution Analysis and Influence of OER

To better understand the influence of pH on the dissolution of Ru, results obtained in SFC-ICP-MS experiments described in previous chapters can be used in further analysis. Visualization of dissolution ratios of anodic and cathodic peaks in both protocols shows a clear trend. The anodic dissolution becomes more dominant with rising pH for each UPL, as captured in Figure 4a–4c. This suggests that an increase in pH can either lead to an oxide layer formation, which is hardly reduced, or the formation of soluble oxides.

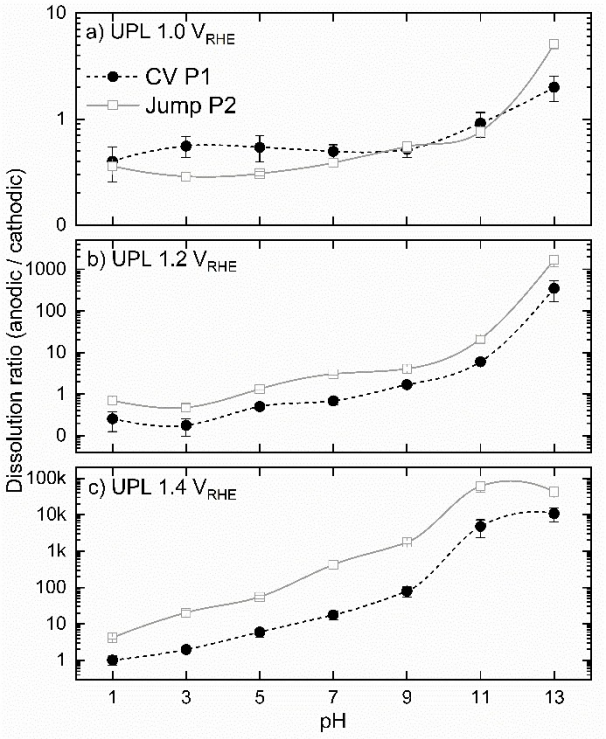

Figure 4. Ratios between anodic and cathodic dissolved amounts in P1 and P2 shown in Figure 1d–f and Figure 3d–f at UPL 1.0 V_{RHE} in a) at UPL 1.2 V_{RHE} in b) and at UPL 1.4 V_{RHE} in c).

Ru is known to be an active catalyst in the OER, and the reaction starts to occur at around 1.3–1.4 V_{RHE}.[50] Considering this, the OER activity can be evaluated from the last CV in P1 (shown in Figure S7) or from the last hold in P2. Figure 5a shows the comparison of current density at 1.4 V_{RHE} for all pHs in P1 (the moment of reaching 1.4 V_{RHE}) and P2 at the end of the potential hold. The current density is lower at the end of the potential hold for all pHs, suggesting decreased activity in OER when exposed to 1.4 V_{RHE} for a longer time. More interestingly, the current density also increases with rising pH in both cases, giving the impression that alkaline pH boosts overall OER activity. The lowest value of the current density reaches 0.1 mA cm^{-2} in P1 (and 0.03 mA cm^{-2} at the end of P2) at pH 1. A similar study investigating the OER activity of RuO_2 across pHs observed the activity trend as follows: pH 1 > pH 12.9 > pH 12.0 > pH 2.8 > pH 6.5, with current density at pH 1 (the highest value) being 0.1 mA cm^{-2} at 1.63 V_{RHE}.[49] Considering that Ru is known to be more active in OER than RuO_2 in both acidic and alkaline environments,[27] we can conclude that the activity observed in this work seems to be in line with the expectations.

The current density itself, however, can be misleading, considering the contribution of Ru dissolution. Ru dissolution is higher than the dissolution of RuO_2, and Ru dissolution is higher in alkaline environments than acidic.[27] This difference in stability during OER can be well visualized by the stability number (S-number) expressed as a ratio between the amount of evolved O_2 molecules (at the measured current density) and the number of dissolved Ru atoms detected by ICP-MS during this process.[51] Figure 5b shows that the S-number is the highest at low pH, suggesting the highest stability of Ru catalyst towards the OER in the acidic environment, where it reaches roughly a 10^3 order of magnitude. In comparison, the stability number of RuO_2 in an acidic environment can vary from 10^2–10^5 orders of magnitude.[52] As Ru is known to be less stable than RuO_2,[27] the values of S-numbers are in line with the literature.

To complete the overall picture of the influence of pH on Ru dissolution, the analysis of the onset of dissolution helps to distinguish the potential at which the process of dissolution

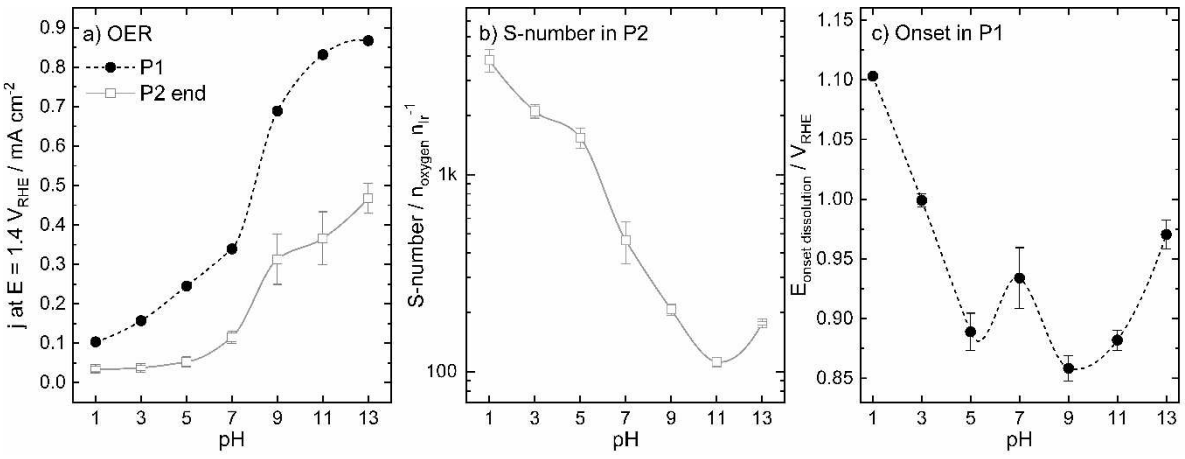

Figure 5. Further analysis from P1 and P2. Current density at UPL 1.4 V_{RHE} in P1 and end of P2 capturing OER at each pH in a). Calculated S-number from the hold at 1.4 V_{RHE} in P2 in b) and the onset of anodic dissolution evaluated from P1 at each pH in c).

started. The first visible dissolution in an anodic sweep is taken against the electrochemical data, as explained in Figure S8 or our previous publication.[53] A higher value of potential, therefore, means that dissolution starts later, and the catalyst is slightly more stable at the higher potential. The values of the onset of dissolutions are plotted against pH in Figure 5c. The dissolution is not observed below 0.85 V_{RHE}, which again suggests that we do not see low potential transitions to Ru^{2+} or Ru^{3+} expected from the Pourbaix diagram, as discussed in Section 3.1. In addition, as observed in our previous studies, the onset of dissolution can be further lowered in the case of the catalyst's dispersion in the form of nanoparticles (0.8 V_{RHE} in acid).[28,33] Based on this analysis, Ru is the most stable at pH 1, while the least stable oneat pH 5 and 9, with a local maximum at pH 7. This unusual behavior can be correlated to buffer capacity, which is the lowest at pH 5 and 9 and highest at pH 7.[54,55] The dissolution at pH 11 and 13 has a lower onset potential than at pH 1 and 3, probably due to the formation of soluble RuO_4^{2-} (see Pourbaix diagram in Figure 2). Interestingly, a similar shape of the curve was also visible in the pH study of Ir.[40]

3. Conclusions

As part of the series exploring the dissolution behavior of noble metals in different pHs, the stability of Ru was studied in a broad pH spectrum using ICP-MS coupled to SFC. Thanks to the rapid oxidation of the Ru surface, a suitable surface treatment was established before this investigation. Potentiodynamic (CVs) and pontentiostatic (holds) electrochemical protocols at different UPLs were used to mimic conditions during the formation of reversible and irreversible oxides or the start of OER. The observed dissolution behavior of Ru at higher potentials ($>$ 0.85 V_{RHE}) was well in line with the thermodynamic predictions of dominant species from the Pourbaix diagram. At lower potentials, on the contrary, we did not observe dissolution due to the formation of predicted soluble Ru^{2+} species. The differences between CVs and holds were also minor, suggesting that thermodynamics seems to have a bigger contribution to dissolution compared to kinetics and that kinetics is relatively fast. Anodic dissolution gradually increased with rising pH, while cathodic dissolution decreased. This phenomenon was only observed for Ru compared to other noble metals such as Pt, Au, and Ir. This suggests that the rising pH either leads to the formation of a hardly reduceable oxide layer or, on the contrary, the formation of highly soluble oxide species (RuO_4^-, RuO_4^{2-}). The stability of Ru decreased exponentially with pH, and amounts dissolved at alkaline pH were especially high at UPL 1.4 V_{RHE}, where OER starts. Even though the OER activity in alkaline was the highest, the low stability number (10^2) jeopardizes the possible application of Ru-based catalysts in OER in alkaline pH at positive potentials. The environments from acidic to neutral are better suited for the OER applications as the formation of soluble RuO_4^{2-} should not occur. On the contrary, the applications of Ru-based catalysts at lower potentials (up to 0.85 V_{RHE}) should not be influenced by the stability issues at any pH, not even in an alkaline environment. The dispersion of catalysts into nanoparticles, however, can further decrease this value. As in the case of more studied metal (Pt), In order to further understand correlations between surface changes of Ru, in-situ surface characterization using synchrotron X-ray-based techniques with the support of DFT calculations would be an interesting addition to future studies.[56,57]

Author Contributions

Mária Minichová: Conceptualization, Data curation, Formal analysis, Investigation, Methodology, Validation, Visualization, Writing – Original Draft, Tatiana Priamushko: Conceptualization, Methodology, Supervision, Validation, Writing – Review & Editing, Matej Zlatar: Conceptualization, Methodology, Validation, Writing – Review & Editing, Karl J.J. Mayrhofer: Funding acquisition, Project administration, Resources, Writing – review & editing, Serhiy Cherevko: Conceptualization, Funding acquisition, Methodology, Project administration, Resources, Supervision, Validation, Writing – Review & Editing

Acknowledgements

This work was funded by the Bavarian Ministry of Economic Affairs, Regional Development and Energy. Open Access funding enabled and organized by Projekt DEAL.

Conflict of Interests

The authors declare no conflict of interest.

Data Availability Statement

The data that support the findings of this study are available from the corresponding author upon reasonable request.

Keywords: Dissolution · Ruthenium · pH · Electrocatalysis · Stability · ICP-MS · Energy conversion

[1] A. G. Elkafas, M. Rivarolo, E. Gadducci, L. Magistri, A. F. Massardo, *Processes* **2023**, *11*, 97.
[2] S. Kazula, S. de Graaf, L. Enghardt, *J. Global Power Propul. Soc.* **2023**, *7*, 43–57.
[3] Y. Wang, Y. Pang, H. Xu, A. Martinez, K. S. Chen, *Energy Environ. Sci.* **2022**, *15*, 2288–2328.
[4] P. Veerakumar, S.-T. Hung, P.-Q. Hung, K.-C. Lin, *J. Agric. Food Chem.* **2022**, *70*, 8523–8550.
[5] R. Manjunatha, A. Schechter, *Electrochem. Commun.* **2018**, *90*, 96–100.
[6] T. Reier, M. Oezaslan, P. Strasser, *ACS Catal.* **2012**, *2*, 1765–1772.
[7] K. A. Stoerzinger, R. R. Rao, X. R. Wang, W. T. Hong, C. M. Rouleau, Y. Shao-Horn, *Chem* **2017**, *2*, 668–675.
[8] M. You, X. Du, X. Hou, Z. Wang, Y. Zhou, H. Ji, L. Zhang, Z. Zhang, S. Yi, D. Chen, *Appl. Catal., B* **2022**, *317*, 121729.
[9] G. Meng, H. Tian, L. Peng, Z. Ma, Y. Chen, C. Chen, Z. Chang, X. Cui, J. Shi, *Nano Energy* **2021**, *80*, 105531.

[10] J. Ohyama, T. Sato, Y. Yamamoto, S. Arai, A. Satsuma, *J. Am. Chem. Soc.* **2013**, *135*, 8016–8021.
[11] Y. Zhou, Z. Xie, J. Jiang, J. Wang, X. Song, Q. He, W. Ding, Z. Wei, *Nat. Catal.* **2020**, *3*, 454–462.
[12] H. A. Gasteiger, N. Markovic, P. N. Ross Jr, E. J. Cairns, *J. Phys. Chem.* **1993**, *97*, 12020–12029.
[13] B. G. Abraham, R. Bhaskaran, R. Chetty, *J. Electrochem. Soc.* **2020**, *167*, 024512.
[14] Y. Kim, H. W. Kim, S. Lee, J. Han, D. Lee, J.-R. Kim, T.-W. Kim, C.-U. Kim, S.-Y. Jeong, H.-J. Chae, B.-S. Kim, H. Chang, W. B. Kim, S. M. Choi, H. J. Kim, *ChemCatChem* **2017**, *9*, 1683–1690.
[15] P. Khanipour, F. D. Speck, I. Mangoufis-Giasin, K. J. J. Mayrhofer, S. Cherevko, I. Katsounaros, *ACS Appl. Mater. Interfaces* **2020**, *12*, 33670–33678.
[16] J. Ying, J.-B. Chen, Y.-X. Xiao, S. I. C. de Torresi, K. I. Ozoemena, X.-Y. Yang, *J. Mater. Chem. A* **2023**, *11*, 1634–1650.
[17] R. Forgie, G. Bugosh, K. C. Neyerlin, Z. Liu, P. Strasser, *Electrochem. Solid-State Lett.* **2010**, *13*, B36.
[18] N. Guruprasad, J. van der Schaaf, M. T. de Groot, *J. Power Sources* **2024**, *613*, 234877.
[19] W. Luo, Y. Wang, C. Cheng, *Mater. Today Phys.* **2020**, *15*, 100274.
[20] H. Wang, Y. Yang, F. J. DiSalvo, H. D. Abruña, *ACS Catal.* **2020**, *10*, 4608–4616.
[21] Y. Wang, G. Wang, G. Li, B. Huang, J. Pan, Q. Liu, J. Han, L. Xiao, J. Lu, L. Zhuang, *Energy Environ. Sci.* **2015**, *8*, 177–181.
[22] S. Cherevko, *J. Electroanal. Chem.* **2017**, *787*, 11–13.
[23] A. R. Zeradjanin, A. A. Topalov, Q. Van Overmeere, S. Cherevko, X. Chen, E. Ventosa, W. Schuhmann, K. J. J. Mayrhofer, *RSC Adv.* **2014**, *4*, 9579–9587.
[24] S. Cherevko, A. R. Zeradjanin, A. A. Topalov, N. Kulyk, I. Katsounaros, K. J. Mayrhofer, *ChemCatChem* **2014**, *6*, 2219–2223.
[25] S. Cherevko, *Curr. Opin. Electrochem.* **2018**, *8*, 118–125.
[26] N. Hodnik, P. Jovanovič, A. Pavlišič, B. Jozinović, M. Zorko, M. Bele, V. S. Šelih, M. Šala, S. Hočevar, M. Gaberšček, *J. Phys. Chem. C* **2015**, *119*, 10140–10147.
[27] S. Cherevko, S. Geiger, O. Kasian, N. Kulyk, J.-P. Grote, A. Savan, B. R. Shrestha, S. Merzlikin, B. Breitbach, A. Ludwig, K. J. J. Mayrhofer, *Catal. Today* **2016**, *262*, 170–180.
[28] A. Kormanyos, P. Büttner, M. Bosch, M. Minichova, A. Körner, K. J. Jenewein, A. Hutzler, K. J. J. Mayrhofer, J. Bachmann, S. Cherevko, *ACS Mater. Au* **2024**, *4*, 286–299.
[29] A. Kormányos, F. D. Speck, K. J. J. Mayrhofer, S. Cherevko, *ACS Catal.* **2020**, *10*, 10858–10870.
[30] D. Escalera-López, S. Czioska, J. Geppert, A. Boubnov, P. Röse, E. Saraçi, U. Krewer, J.-D. Grunwaldt, S. Cherevko, *ACS Catal.* **2021**, *11*, 9300–9316.
[31] L. Gancs, N. Hakim, B. Hult, S. Mukerjee, *ECS Trans.* **2006**, *3*, 607.
[32] P. Jovanovič, V. S. Šelih, M. Šala, S. Hočevar, F. Ruiz-Zepeda, N. Hodnik, M. Bele, M. Gaberšček, *Electrochim. Acta* **2016**, *211*, 851–859.
[33] M. Minichová, T. Priamushko, A. Hutzler, T. Hrbek, I. Khalakhan, K. J. J. Mayrhofer, S. Cherevko, *Electrochim. Acta* **2024**, *502*, 144764.
[34] M. Schalenbach, O. Kasian, M. Ledendecker, F. D. Speck, A. M. Mingers, K. J. J. Mayrhofer, S. Cherevko, *Electrocatalysis* **2018**, *9*, 153–161.
[35] M. Zhang, J. Chen, H. Li, P. Cai, Y. Li, Z. Wen, *Nano Energy* **2019**, *61*, 576–583.
[36] L. Zhang, L. Wang, Y. Wen, F. Ni, B. Zhang, H. Peng, *Adv. Mater.* **2020**, *32*, 2002297.
[37] L. Zhang, H. Jang, H. Liu, M. G. Kim, D. Yang, S. Liu, X. Liu, J. Cho, *Angew. Chem.* **2021**, *133*, 18969–18977.
[38] J. Chen, C. Chen, M. Qin, B. Li, B. Lin, Q. Mao, H. Yang, B. Liu, Y. Wang, *Nat. Commun.* **2022**, *13*, 5382.
[39] J. Mahmood, F. Li, S.-M. Jung, M. S. Okyay, I. Ahmad, S.-J. Kim, N. Park, H. Y. Jeong, J.-B. Baek, *Nat. Nanotechnol.* **2017**, *12*, 441–446.
[40] M. Zlatar, D. Escalera-López, C. Simon, V. Briega-Martos, K. Stojanovski, S. Cherevko, *Electrochim. Acta* **2025**, *513*, 145450.
[41] V. Briega-Martos, K. Stojanovski, M. Zlatar, C. Göllner, S. Cherevko, *Electrochim. Acta* **2024**, *501*, 144793.
[42] K. Stojanovski, V. Briega-Martos, M. Zlatar, C. Göllner, S. Cherevko, *ChemElectroChem* **2024**, *11*, e202400373.
[43] B. Łosiewicz, M. Martin, C. Lebouin, A. Lasia, *J. Electroanal. Chem.* **2010**, *649*, 198–205.
[44] A. Mechler, A. Topalov, I. Katsounaros, S. Klemm, K. Mayrhofer, *J. Electrochem. Soc.* **2012**, *159*, F670–F675.
[45] M. L. B. Rao, A. Damjanovic, J. O. M. Bockris, *J. Phys. Chem.* **1963**, *67*, 2508–2509.
[46] J. Juodkazytė, R. Vilkauskaitė, B. Šebeka, K. Juodkazis, *Trans. IMF* **2007**, *85*, 194–201.
[47] I. Povar, O. Spinu, *J. Electrochem. Sci. Eng.* **2016**, *6*, 145.
[48] M. Pourbaix, *Atlas of Electrochemical Equilibria in Aqueous Solutions*, NACE **1966**.
[49] D.-Y. Kuo, H. Paik, J. Kloppenburg, B. Faeth, K. M. Shen, D. G. Schlom, G. Hautier, J. Suntivich, *J. Am. Chem. Soc.* **2018**, *140*, 17597–17605.
[50] S. B. Scott, R. R. Rao, C. Moon, J. E. Sørensen, J. Kibsgaard, Y. Shao-Horn, I. Chorkendorff, *Energy Environ. Sci.* **2022**, *15*, 1977–1987.
[51] S. Geiger, O. Kasian, M. Ledendecker, E. Pizzutilo, A. M. Mingers, W. T. Fu, O. Diaz-Morales, Z. Li, T. Oellers, L. Fruchter, A. Ludwig, K. J. J. Mayrhofer, M. T. M. Koper, S. Cherevko, *Nat. Catal.* **2018**, *1*, 508–515.
[52] C. Wei, Z. Wang, K. Otani, D. Hochfilzer, K. Zhang, R. Nielsen, I. Chorkendorff, J. Kibsgaard, *ACS Catal.* **2023**, *13*, 14058–14069.
[53] M. Minichová, C. Van Pham, B. Xiao, A. Savan, A. Hutzler, A. Körner, I. Khalakhan, M. G. Rodríguez, I. Mangoufis-Giasin, V. Briega-Martos, A. Kormányos, I. Katsounaros, K. J. J. Mayrhofer, A. Ludwig, S. Thiele, S. Cherevko, *Electrochim. Acta* **2023**, *444*, 142032.
[54] T. Nishimoto, T. Shinagawa, T. Naito, K. Takanabe, *ChemSusChem* **2021**, *14*, 1554–1564.
[55] W. M. Haynes, *CRC Handbook of Chemistry and Physics*, CRC press **2016**.
[56] T. Fuchs, J. Drnec, F. Calle-Vallejo, N. Stubb, D. J. S. Sandbeck, M. Ruge, S. Cherevko, D. A. Harrington, O. M. Magnussen, *Nat. Catal.* **2020**, *3*, 754–761.
[57] T. Fuchs, V. Briega-Martos, J. Drnec, N. Stubb, I. Martens, F. Calle-Vallejo, D. A. Harrington, S. Cherevko, O. M. Magnussen, *Angew. Chem.* **2023**, *135*, e202304293.

Manuscript received: November 28, 2024
Revised manuscript received: February 26, 2025
Version of record online: April 3, 2025